Biochimica et Biophysica Acta, 777 (1984) 9–20
Elsevier

BBA 72224

A 12 Å RESOLUTION X-RAY DIFFRACTION STUDY OF THE PROFILE STRUCTURE OF ISOLATED BOVINE RETINAL ROD OUTER SEGMENT DISK MEMBRANES

DONATELLA PASCOLINI [a], J. KENT BLASIE [a] and SOL M. GRUNER [b]

[a] *Departments of Chemistry and Biochemistry / Biophysics, University of Pennsylvania, Philadelphia, PA 19104 and* [b] *Department of Physics, Princeton University, P.O. Box 708, Princeton, NJ 08540 (U.S.A.)*

(Received January 9th, 1984)
(Revised manuscript received May 1st, 1984)

Key words: Disk membrane; X-ray diffraction; (Bovine retina)

Electron density profiles of disk membranes isolated from bovine retinal rod outer segments have been determined to 12 Å resolution by analysis of the X-ray diffraction from oriented multilayers, in the absence of lipid phase separation. Data were collected on both film and a two-dimensional TV-detector; both detectors yielded identical patterns consisting of relatively sharp lamellar reflections of small mosaic spread. The unit cell repeat was reversibly varied over the range of 143 to 183 Å. The diffraction patterns changed dramatically at 150 Å; consequently, the low (less than 150 Å) and high (greater than 150 Å) periodicity data were independently analyzed via a swelling algorithm. The high periodicity data yielded two statistically equivalent phase choices corresponding to two symmetric, but different membrane profiles. The low periodicity data yielded essentially one, characteristically asymmetric profile. These profiles have been modeled with regard to the separate profiles of rhodopsin, lipid and water, subject to the known composition of the isolated disk membranes.

Introduction

Vertebrate visual excitation begins with the absorption of light by the photoreceptor membrane in the outer segment of retinal rods and cones. Intact rod outer segments have been the subject of numerous investigations aimed at determining the ultrastructure of the photoreceptor membrane (see Ref. 1 for a review). Since the rod outer segment is a naturally periodic stack of flattened membranes vesicles, called disks, it is well suited for investigations by X-ray and neutron diffraction. Unfortunately, irregularities in the widths of the fluid spaces between the disk membranes limit the resolution of the lamellar diffraction data to about 25 Å [2]. (Resolution throughout this paper is defined as $\lambda/2 \sin \theta_{max}$ where $2\theta_{max}$ is the maximum diffraction angle for which lamellar data were obtained). The lack of detail in the electron density profiles obtained from such data at this resolution has not permitted unambiguous modelling of the membrane in terms of its major components. An alternative approach to obtaining the diffraction data is to isolate the disks from the rod and artificially stack them into an oriented multilayer [3,4]. The purposes of this method are two-fold. First, the fluid layers in the multilayer can be readily manipulated by controlled hydration and dehydration. This has the consequence of greatly reducing the various forms of disorder in the multilayer lattice and yielding lamellar diffraction to much higher resolution [5–7]. Second, isolated disks can be labelled and the effects can be observed in the diffraction patterns. The process of dehydration, however, can also lead to phase separation phenomena which produce diffraction

characterized by more than one set of Bragg lattices. This problem, often encountered with membranes, precludes a meaningful structure determination, as the diffraction arises from an altered membrane of non-unique composition. The process of phase separation in rod outer segment multilayers has been investigated [8,9] and is known to culminate in coexisting domains of hexagonal (H_{II}) and lamellar phases within the specimen [7].

Lamellar diffraction data from highly hydrated, isolated disk multilayers in the absence of lipid phase separation have been recently presented [9]. This data exhibited the effects of lattice disorder which limited the resultant profiles to 30 Å resolution. It was evident, however, that the lattice disorder was highly dependent on the specimen preparation. We have refined the specimen preparation and data collection methods and have now obtained lamellar diffraction to 12 Å resolution over a periodicity range (140–180 Å) in the absence of lipid phase separation. The collection and analysis of the X-ray diffraction is presented below.

Methods

Preparation of disk membrane dispersions and multilayers

All operations were performed under dim red light at 4°C. At every stage of the procedure, care was taken to minimize oxidative damage of the membranes: all solutions were deoxygenated and purged with argon. Membrane dispersions and multilayers were kept under argon or helium. Fresh bovine eyes were obtained from a slaughterhouse and dissected within 6 h. Rod outer segments were isolated according to the sucrose flotation procedure of Raubach et al. [10,11]. The rod outer segment membranes collected by centrifugation after the second flotation were resuspended in 68 mM sodium phosphate buffer containing 0.1 mM EDTA and 0.15 mM $CaCl_2$, at pH 7.0, and directly dialyzed for 24 h against a 250-fold vol. water, containing 0.1 mM EDTA and 0.1 mM dithiothreitol. The membranes were then gently centrifuged (7000 × *g* for 10 min) and the soft pellet was resuspended in 68 mM sodium phosphate buffer (0.1 mM EDTA, 0.15 mM $CaCl_2$, 0.1 M NaCl, 0.1 mM dithiothreitol, pH 7.0). This buffer was also used during sedimentation in the formation of the multilayer. The purity of final disk suspension was checked by the absorbance ratio at 280/500 nm. Lipid peroxidation was assayed by measuring the 250/280 nm ratio [12]. The values for these ratios were typically 2.0–2.5 and 0.5, respectively. SDS-polyacrylamide gel electrophoresis indicated that the predominant protein in the preparation was rhodopsin.

Multilayers were formed by sedimenting an aliquot of disk dispersion containing 0.25 mg rhodopsin onto aluminum foil strips (2 h at 80 000 × *g*) in sedimentation cells as described previously [3,4]. The foil strip bearing the thin, 5 mm diameter pellet was tightly wrapped around cylindrical aluminum or glass slides (1.3–2.1 cm radius). The pellets were partially dehydrated with two alternative procedures: the wet pellets were directly mounted in the specimen chamber and equilibrated by a humidity generator (see below) or slowly dried in a sealed bottle over a saturated solution of $NH_4H_2PO_4$ (relative humidity = 93%). Specimens were mounted in the X-ray specimen chamber with minimal (less than 1 min) exposure to air and immediately purged with moist helium.

Instrumentation

Ni-filtered CuK_α ($\lambda = 1.54$ Å) X-rays were generated on a Rigaku RU-200 Rotaflex rotating anode generator (50 kV, 55 mA) and collimated and focused using slits and single mirror Franks optics, as described previously [13]. X-ray diffraction was recorded on a quantum-limited image-intensifier area detector, as described previously [14]. Diffraction was also recorded on film using line focus via the equipment described previously [15]. In all cases, the X-ray beam was directed to tangentially graze the surface of the multilayer.

Data collection

All X-ray experiments were performed at 4°C on dark adapted rod outer segments. The camera alignment and specimen geometry have been described previously (see, for example, Ref. 15).

Detector data. A programmable humidity generator [16] was used to regulate the relative humidity inside the specimen chamber by means of a stream of moist helium. Regulation was obtained over a wide range of humidities and varying from 90%

relative humidity to well above saturation by isobaric injection of gas at a given dewpoint into the cold specimen chamber. The advantage of the humidity generator is that it allows continuous and reversible variation of the specimen water content. Since specimens varied in the rate at which they dehydrated, the real-time progress of the dehydration was monitored by using the fast X-ray detector to determine the multilayer repeat spacing. Typically, a continuous sequence of alternating short (less than 10 s) and long (less than 5 min) X-ray exposures were taken. This method of data collection produces a series of complete diffraction patterns, each corresponding to a hydration state of the multilayer. In effect, it produces an extremely fine swelling experiment that can be reversed a few times within a few hours. The patterns can be displayed at any time on a television screen and the evolution of the diffraction can be closely observed. Typically, the strongest X-ray reflections were 2–3 orders of magnitude more intense than the weakest ones. The X-ray detector is of the integrating type and saturated locally when over-exposed to an intense reflection. By alternating short and long exposures, one could obtain unsaturated patterns of strong reflections and good quantum statistics on weaker ones on a time-scale that was still short relative to the evolution of the specimen. Short and long exposures could later be merged by scaling by the exposure time. Exposures which exhibited no significant evolution of the specimen were digitally summed. Diffraction images from the detector were stored on computer disk as two-dimensional arrays of 256×256 elements.

Film data. X-ray film exposures were recorded for 8–18 h on Kodak No-Screen film using a cylindrical cassette at 62.5 mm from the specimen (high angle exposures) or flat cassettes at distances ranging to 250 mm (low angle exposures). Specimens were equilibrated either with the humidity generator or, in instances when the generator was unavailable, with saturated salt solutions. In the latter case, multilayers were stored overnight over saturated salt solutions and then transferred to the X-ray chamber. By substituting gas washing bottles containing different salts, the relative humidity could be step-wise varied from 90 to 98%. Typically, a small cup of the saturated salt solution was also placed inside the X-ray chamber next to the specimen. As the samples were sensitive to even small changes in the humidity, care was taken to keep the specimen chamber and the gas washing bottle at the same temperature.

Data reduction and analysis

Detector data was first corrected for known detector transfer function effects as described previously [13]. The two-dimensional data were angularly integrated onto the lamellar axis (see Fig. 1),

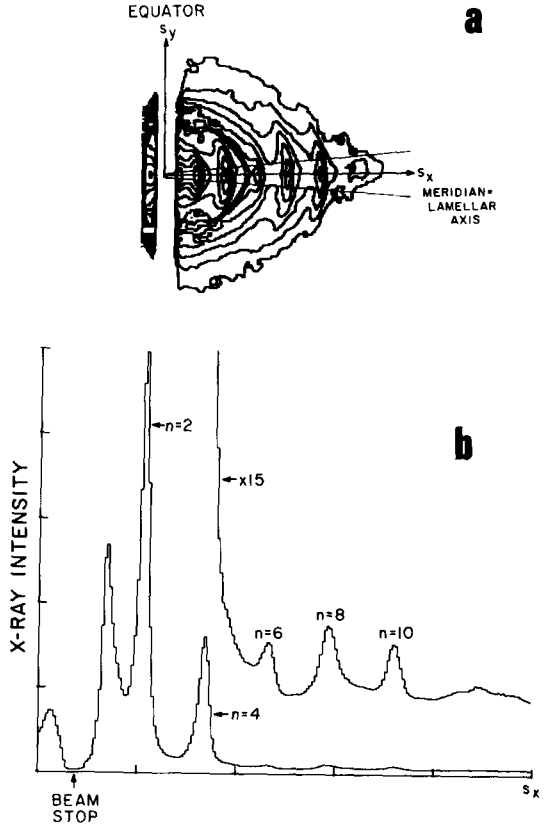

Fig. 1. (a) A diffraction pattern of an isolated rod outer segment disk multilayer, in equilibrium. Lamellar Bragg orders $n = 2, 4, 6, 8, 10$ and 12 from a unit cell of 164 Å are visible. This exposure was acquired in 20 min on the TV-detector. The contour levels shown were chosen to clearly display the orders. (b) If the data between the lines at $\pm 5°$ to the meridian in (a) are integrated as a function of distance from the origin of diffraction (behind the beam stop), one obtains the graph of the lamellar diffraction shown. The peak immediately to the right of the beam stop is camera scatter. In all figures displaying X-ray intensity vs. s, the X-ray intensity is in arbitrary units.

yielding a one-dimensional record of total counts vs. the reciprocal coordinate s ($s \equiv 2(\sin\theta)/\lambda$, where $2\theta \equiv$ diffraction angle), in steps of $\Delta s \approx 2.5 \cdot 10^{-4}$ Å^{-1}. The short exposure records were scaled by the ratio of long to short exposures times and merged with the long exposures records about point which were midway between unsaturated reflections. Sequentially acquired records spanning times over which no significant specimen evolution occurred were summed as needed. Film data were densitometrized with a Joyce-Loebl microdensitometer scanning along the lamellar axis through the center of each reflection; the slit dimensions were fixed at a height of 0.5 and 0.03 mm width. Background-corrected, integrated peak intensities and peak centers were computed by the method described in Ref. 17. Periodicities were determined from the slope of a stright line fit to the peak center positions vs. s. A Lorentz correction proportional to s was applied in all cases. This was warranted for the detector data due to the angular integration and X-ray geometry. In the case of the film data, all the reflections up to $2\theta_{max}$ exhibited very little mosaic spread; no microdensitometer correction due to scanning with a slit of fixed height was therefore necessary.

Electron density profiles were derived using the swelling algorithm of Stamatoff and Krimm [18].

Results

Raubach et al. [10,11] did extensive electron microscopy studies showing that the slow, low-salt dialysis gently isolates disks of a uniform size, compatible with the mean size of the disks within the intact rod, and of uniform sidedness. They observed that the disks appeared non-inverted with respect to native rod outer segments disks. The preparation used for this work is essentially identical to the one used for the studies mentioned above; only a few changes were introduced, as they appeared to be helpful in obtaining reproducible high quality diffraction patterns. Washing the membranes with water before dialysis was eliminated (as very drastic) and the precautions described by Stone et al. [12] were rigorously applied in order to avoid lipid peroxidation (tested at the beginning and at the end of the experiments, the ratio of absorbance at 250 and 280 nm was found to be routinely constant). Freeze-fracture electron microscopy performed on the disk dispersions (Costello, M.J., Pascolini, D., Gruner, S.M., unpublished data) indicated the vesicles to be predominantly unilamellar with sidedness preservation. The electron micrographs appeared very similar to those shown in Ref. 19.

Evolution of the X-ray diffraction

Immediately after centrifugation, the multilayers exhibit weak, relatively unsampled lamellar diffraction (see the first trace of Fig. 2), indicative of widely varying widths of the fluid spaces between the membranes. As water is progressively evaporated from the oriented multilayer, lamellar reflections from a well-defined Bragg lattice appear and grow in intensity. Concomitantly, the reflections sharpen and move away from the diffraction origin ($2\theta = 0$) as the unit cell shrinks. Initially, when the sample is still equilibrating (see Fig. 2c), all orders of the Bragg lattice are visible; however, as the equilibration proceeds, the odd-in-

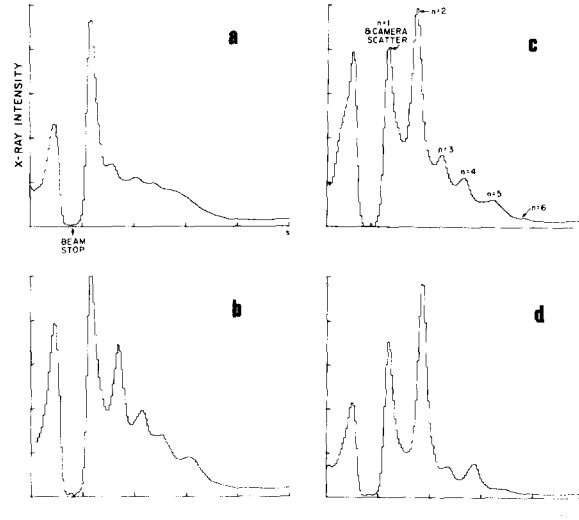

Fig. 2. The development of the lamellar reflections is seen in this sequence of integrated TV-detector patterns taken on a dehydrating rod outer segment disk multilayer in Ringers containing 6% sucrose (by weight). (a) is the most hydrated and (d) is the least hydrated. The first-order is not distinguishable from the camera scatter in these exposures, but may be clearly seen in other exposures (not shown). Note that by (d), the odd-indexed orders have almost disappeared. Lattice spacings for (a) to (d) are 261, 204, 185 and 178 Å, respectively, i.e., the high d regime.

dexed orders fall in intensity relative to the even orders (Fig. 2d) and eventually become too weak to be measured (Fig. 1b).

Fig. 3. illustrates the lamellar diffraction typically exhibited by fully equilibrated multilayers with unit cell repeats in the range of 180 to 150 Å. The diffraction, which extends to about $(12\ Å)^{-1}$, contains sharp regularly spaced reflections that correspond to the even orders of the Bragg lattice with negligible odd orders. In these patterns, the background scattering is very weak compared to the lamellar diffraction and it appears due solely to the characteristics of the camera, the intensity maxima are observed on a nearly flat background. The width of the reflections remains nearly constant to 2 θ_{max} with no measurable broadening at high angle. The multilayer appears, therefore, to be well-oriented, and not significantly affected by lattice or substitution disorder. The mosaic spread, or lattice misorientation, which would produce arcing of the reflections, is small (Fig. 1 and Fig. 3). In the high-angle region, diffuse primarily equatorial $(10\ Å)^{-1}$ (Fig. 3a) and meridional $(5\ Å)^{-1}$ (not shown) diffraction are observed; this is usually taken as indicative of α-helical polypeptide

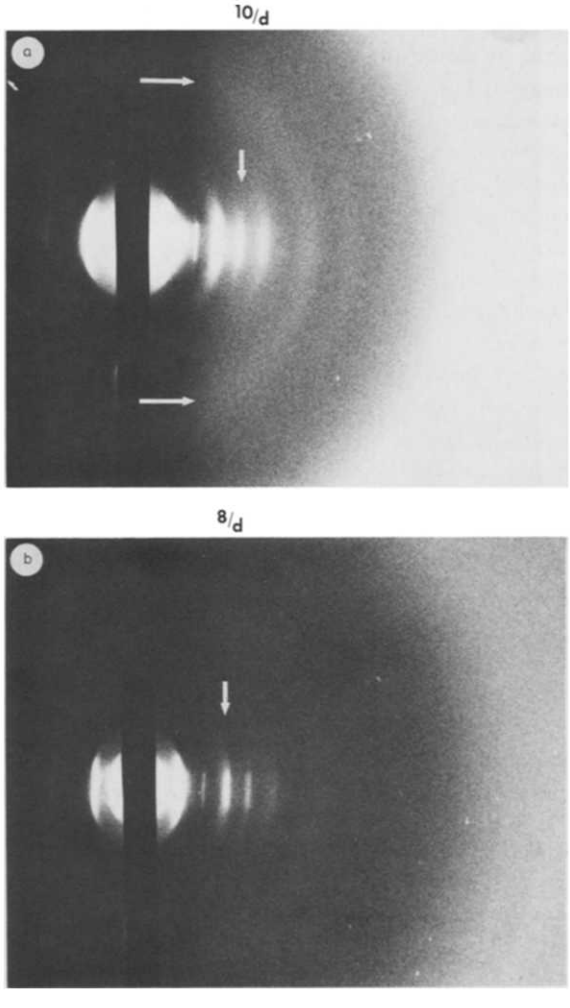

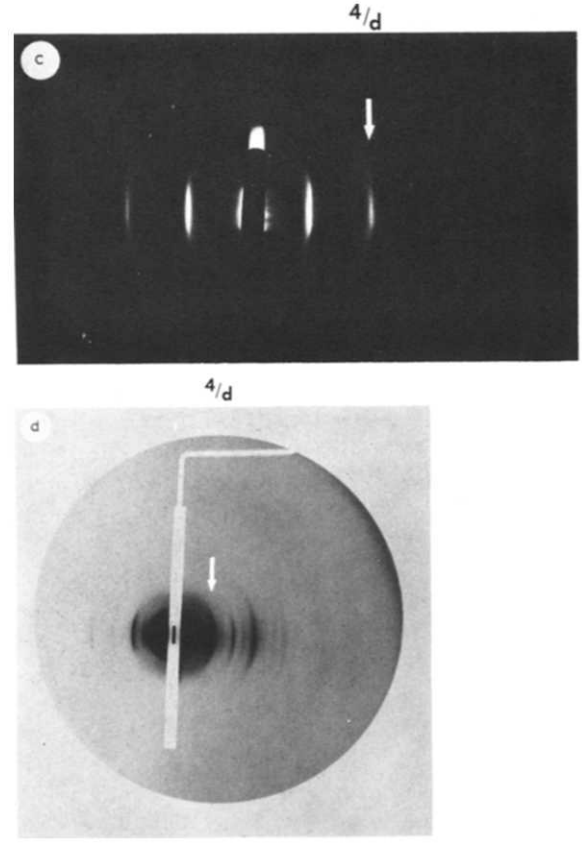

Fig. 3. (a, b) Reproductions of X-ray diffraction patterns recorded on film. The 1st film (a) and 2nd film (b) are from an isolated disk multilayer specimen of 160 Å periodicity. Orders 2, 4, 6, 8, 10 and 12 are spaced along the (horizontal) meridian. Also note the diffuse equatorial scatter (horizontal arrows) at 10 Å in (a). The films were mounted in a cylindrical cassette at 62.5 mm from the specimen. Exposure time = 17 h. (c) A low-angle pattern from the same specimen under the same conditions as in (a and b). Orders 2 and 4 are seen. The flat film cassette was 250 mm from the specimen. Exposure time = 6 h. (d) A low-angle pattern (14 h exposure) from a specimen which has a periodicity of 140 Å. Orders 1 and 2 are overexposed on the 1st film shown, but 3, 4, 5, 6, 7, 8, 9, 10 and 11 may be seen. See text. From a flat cassette at 135.6 mm from the specimen.

columns oriented generally perpendicular to the membrane plane [20,21].

The diffraction patterns from fully equilibrated multilayers, as previously described [9], change greatly as the periodicity decreases further below 150 Å. First, the $n = 1$ reflection brightens. This is followed, in succession, by $n = 3$ and then the remaining odd-indexed orders (Fig. 3d). Throughout, no dramatic or discontinuous changes occur in the intensity of the even orders or the high-angle features. The mosaic spread and lattice disorder are also unchanged. This situation is reversible: the specimens can be subjected to water vapor pressures above saturation and assume their earlier characteristic diffraction and unit cell dimensions. Over the full range of periodicities described above, the reversible hydration-dehydration of the multilayer does not produce lipid phase separation in the multilayer; if, however, the specimens are allowed to shrink even further ($d < 140$ Å, not shown), additional reflections appear on the meridian in between the existing orders which cannot be indexed on the same lattice, indicating that the specimen has undergone lipid phase separation. In the case of extreme dehydration of the multilayer, $d \approx 120$ Å, off-meridional reflections also appear, indicative of the formation of so-called H_{II} lipid domains in the multilayer [7]. These processes appear to be irreversible; in fact, the multilayer does not swell even when subjected to extremely high water vapor pressures.

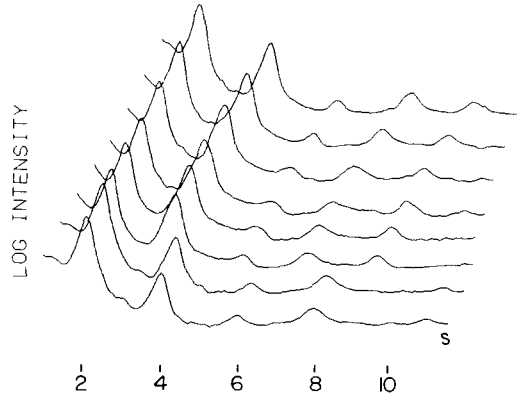

Fig. 4. Lamellar diffraction from a single specimen taken over a course of a day as the specimen was hydrated and dehydrated. The log X-ray intensity vs. s is shown as derived from integrations through six TV-detector exposures. The lattice periodicities are, from top to bottom, 157.4, 160.6, 164.8, 164, 163.8, 149, 145 and 143 Å. The 143 and 145 Å pair were used to compute the low periodicity profiles of Fig. 6. The 149–165 Å data were used to compute the high periodicity profiles of Fig. 5.

The evolution of the diffraction of a specimen, as described above, is summarized in Fig. 4: each trace represents the logarithm of the integrated intensity of lamellar diffraction at various periodicities. These data were collected from a single specimen via the area detector.

Discussion

Interpretation of the lamellar diffraction: lattice structures

Real-time two-dimensional X-ray detection, coupled with humidity control, provides insight to the evolution of the lattice structure of the membrane multilayers. Continuous changes in the diffraction patterns can be monitored over a large range of humidities and the characteristics of each pattern can be interpreted. At the early stages of equilibration of the multilayer, the lamellar diffraction is consistent with the behavior expected from osmotically equilibrating, flattened, closed vesicles. Consider the unit cell profile as the centrosymmetric, projected electron density distribution which spans the center of one disk to the center of the next (two membrane profiles per unit cell [2]). Both strong odd- and even-indexed reflections are expected if each half of the unit cell profile is, itself, neither symmetric nor antisymmetric. This is because, in this case, the Fourier decomposition of each half of the unit cell profile has both non-zero sine and cosine terms. It is known from experiments on intact rod outer segments [22] and isolated disks [9] that the electron density profile of the disk membrane is, at low resolution, very nearly centrosymmetric. Each half of the unit cell would be asymmetric if the disk membranes were placed off-center in the half unit cell, i.e., if the intra- and interdiskal fluid spaces were of unequal width. As the fluid spaces equalize, the half unit cell would look more and more symmetric, leading to the decrease in intensity of the odd-indexed orders. This effect may be enhanced by centrifuging the disks in buffer containing a few percent sucrose: since sucrose can cross the disk vesicle wall only very slowly, the rate at

which the intravesicle fluid comes to equilibration with the intervesicle fluid is slowed. The osmotic effect is to reduce the intravesicle fluid spaces relative to the intervesicle space. As time proceeds, sucrose is presumed to cross the membrane and the fluid spaces equalize with the concomitant smooth decrease in intensity of the odd-indexed orders (Fig. 2).

The observations described above allow interpretation of the equilibrium states of the multilayer achieved when the humidity is fixed at a high value. In these cases, ambiguity could arise regarding the dimension of the unit cell, as the patterns might be interpreted as arising from reflections placed at $1/d$, $2/d$,... $Å^{-1}$ ($d = 90$–75 Å, according to the particular pattern considered) and could indicate a unit cell of 90–75 Å composed by a single membrane profile. The behavior of the diffraction during equilibration, however, strongly suggests that those reflections are instead the even-order reflections of a Bragg lattice at $1/d$, $2/d$, $3/d$,... ($d > 180$ Å) which has smoothly evolved into reflections at $2/d$, $4/d$,... ($150 < d < 180$). The decrease in intensity of the odd orders during the equalization of the fluid layers culminates with the disappearance of the odd orders when the inter- and intravesicle spaces, between membranes of nearly symmetric electron density profiles, are identical. The unit cell profile, thus, contains two membrane profiles and is formed from a vesicle in which adjacent membranes alternate in the vectorial orientation of the external disk surfaces.

This conclusion is further supported by the continued multilayer behavior as d decreases below 150 Å: reflections are now observed at $1/d$, $2/d$, $3/d$,..., $11/d$, $d \approx 150$ Å, i.e., all the reflections from a lattice whose unit cell profile contains two membranes. We offer an interpretation of these phenomena in the following scheme, which summarizes the evolution of the lattice structure:

(1) The isolated disk membrane profile to 12 Å resolution, is nearly symmetric in its electron density distribution but asymmetric in its chemical properties, i.e., the disk has a chemically distinct inside and outside.

(2) A freshly spun disk multilayer consists of flattened, closed vesicles of widely varying fluid spaces between the membranes, giving rise to lamellar diffraction characteristic of a highly disordered multilayer lattice. The diffraction is largely confined to the meridian; therefore, the vesicles are somewhat flattened.

(3) As dehydration proceeds, the inter- and intravesicle fluid spaces equalize in width. The intensity of the odd-order lamellar reflections falls relative to the even-indexed orders. This process can be slowed by the addition of bulky solute to the intervesicle fluid.

(4) As the multilayer comes to equilibrium with the applied water vapor pressure, and as the unit cell (two membranes) repeat d approaches 180 Å, the longer range forces between the membranes act to center each membrane with respect to its neighbors. The intensity of the odd-indexed orders (to a 12 Å resolution) falls to negligible values as the specimen equilibrates.

(5) As d falls below 150 Å, the forces between the membranes become dominated by the close-range interactions which are characterically different, for chemically different surfaces [23]. This asymmetrizes the unit cell electron density profile. Three, not mutually exclusive possibilities exist: (a) The inter- and intravesicle fluid widths are no longer equal. (b) The membrane profile has been altered by movement of mass perpendicular to the membrane plane. (c) Interdigitation of surface features has occurred preferentially on one surface of the disk.

(6) Below 140 Å, the membranes undergo lipid phase separation; the nature of phase separation just below 140 Å is not known.

(7) The very low hydration effects are characterized by well-defined phase separated domains of H_{II} phase embedded in a predominant lamellar phase [7]. The lamellar phase 'bottoms out' at about $d = 118$–120 Å when vacuum-dried. Throughout, the $1/10$ and $1/5$ $Å^{-1}$ reflections are strongly present, indicating that the α-helix orientiation remains predominantly perpendicular to the membrane planes.

This picture of events is entirely consistent with earlier studies [7–9].

Phasing of the lamellar diffraction

The swelling algorithm developed by Stamatoff and Krimm [18] was applied separately to the high ($150 \leqslant d \leqslant 180$) and low ($140 < d < 150$) periodic-

ity data collected via the area detector to calculate the unit cell electron density profiles. We would emphasize the absence of lipid phase separation phenomena in these multilayers over this entire range of periodicities ($140 < d < 180$ Å) utilized. In both cases, as previously discussed, the unit cell profile is composed by a membrane pair with a mirror plane of symmetry. The applicability of the algorithm within each range of periodicities is guaranteed by the following factors. First, because data were collected continuously as the water content of the unit cell was slowly varied, pairs of data sets were available from multilayer periodicities which differed by only a few angstroms. The swelling algorithm was applied to such data set pairs. In the limit as the difference in the unit cell repeats of a pair approaches zero, it is reasonable to assume that only the widths of the fluid spaces between the membranes have changed. Second, the lattice disorder effects were not appreciable, consistently, in all the patterns and could be ignored. Thus, integrations of the area of the nth reflection, which was relatively sharp throughout, could be assumed as the integrated reflection intensity at n/d.

Given two sets of integrated lamellar reflection intensities corresponding to two different multilayer periodicities, the method of analysis involves the calculation of two electron density profiles, $\rho(z)$, related by:

$$\rho_1(z) = A\rho_2(z) + B$$

where A is a scale factor, B is a factor associated with the unobservable origin reflections and z is an axis perpendicular to the membrane plane. Pairs of profiles are compared for all possible phase combinations for the reflections. The correct phase combination should provide the same $\rho(z)$ for both periodicities. A statistical parameter, Δ, computed for each phase combination pair, measures the smallest least-square difference between the two profiles and is used to select the most probable phase combination pair.

When applied to the high periodicity (greater than 150 Å) data pairs of Fig. 4 at a resolution of 15–16 Å, all but two phase assignments can be eliminated, the same two for all the pairs considered. These two assignments and the corresponding profiles are shown in Fig. 5 for the 160.6 and 163.8 Å periodicity data sets. For each pair of periodicities, the errors in $\rho(z)$ and consequently in Δ, are dominated by the experimental errors in the weakest orders of the lamellar diffraction. In the error analysis presented by Stamatoff and Krimm [18] with the swelling algorithm, 10% errors in the intensities induce large deviation in Δ, of about 30–40%. In our case, the differences of not more than 1% in Δ cannot then be considered significant, since the errors in the weaker, higher angle reflections are of the same magnitude, not more than 1%, as determined via the algorithm used to calculate the integrated intensities. Thus, we cannot distinguish between the two most probable phase combinations above. All other phase combinations possessed Δ values differing from

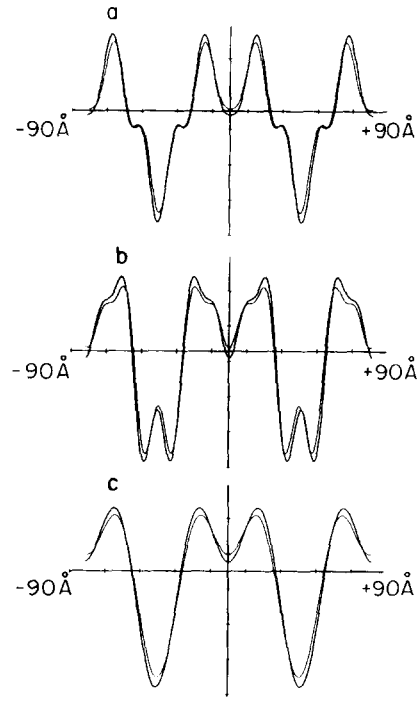

Fig. 5. Unit cell electron density profiles, $\rho(z)$, are shown for the high periodicity data pair ($d = 160.6$ and 163.8 Å) of Fig. 4. (Figs. 5 and 6 all show electron density profiles. In each case, the abscissa is z, in angstroms, one division = 20 Å, and the ordinate is $\rho(z)$, in arbitrary units of electron density.) The two traces shown superimposed in each figure are $\rho_1(z)$ and $\rho_2(z)$ of Eqn. 1. The profiles shown in (a) and (b) fit the data equally well, as judged by the statistical measure, Δ. The phases for the orders $n = 2, 4, 6, 8, 10$ are in (a) 1, −1, −1, −1, 1 and in (b) 1, −1, −1, 1, −1, respectively. If the data are artificially truncated after the 6th order, the profile, (c), results.

those of the two most probable by more than 10%.

The swelling algorithm was applied also to the data collected on film and the same two phase combinations were selected. These two phase assignments, thus obtained independently for several data pairs over a wide range of periodicities, appear to be the two most probable for the high periodicity data. The phases obtained for each order, according to the two most probable phase combinations, for the high periodicity data are reported in Table I ($183 \leqslant d \leqslant 149$ Å). Note that the two phase combinations differ only in the phases of the 8th and 10th order. If the data are artificially truncated at the minimum between the 6th and 8th order, only the low resolution (approx. 30 Å) profile of Fig. 5c is obtained. This truncation provides a profile which compares directly, in terms of resolution, with the profiles obtained for disks in the intact rod and with the profiles of Gruner et al. [9], obtained via a different preparation of the isolated disks and different data analysis procedure.

As mentioned earlier in this section, the data at low periodicity (i.e., data with $140 < d < 150$ Å) containing both, odd and even orders, were phased separately; that is, pairs formed by one data set at high periodicity and one at low periodicity were not considered. We have discussed earlier how the presence of odd-indexed orders can be explained in terms of changes in the lattice. We indicated that such changes do not imply drastic transformation of the membrane itself. Even so, the structure factor of the unit cell (membrane pair) profile at high and low periodicity is not invariant as required by the swelling methods of phasing. Consequently, one cannot apply the swelling procedure to a data set pair composed of a low and a high periodicity data set. Within the range of low periodicities, however, and as $\Delta d \to 0$, swelling methods are legitimate. Applied to the low periodicity data at 12 Å resolution, two statistically indistinguishable phase choices are obtained, the corresponding profiles are shown in Fig. 6. The phase choices differ only in the assignment of sign for the very weak 3rd order (see Table I, $d = 145$ and 143 Å), thus yielding two essentially identical profiles. For these data also, a truncated low resolution (approx. 30 Å) profile was obtained and it is shown in Fig. 6c.

It is of interest to compare the low and high periodicity phase choices. The low periodicity choices (Fig. 6a, b) differ from the phases of Fig. 5a in the 10th order and from Fig. 5b in the 8th, all the other phases being the same. Moreover, it is observed that the intensity of the 10th order goes through zero in the vicinity of $d = 150$ Å (data not shown) as d varies from 143 to 157 Å. Consequently, it may be argued that the 10th order intensity has undergone a phase reversal between the low and high periodicity regimes. By contrast,

TABLE I

PHASE ASSIGNMENTS FOR UNIT CELLS WITH PERIODICITIES RANGING FROM 183 TO 143 Å, ORDERS AT $s \approx n/d$

Blank phases indicate that the intensity of the order was insignificant; note that the phases for $n = 8$ and $n = 10$ are either -1, $+1$ or $+1$, -1, respectively, for $d > 156$ Å.

d(Å)	$n=1$	$n=2$	$n=3$	$n=4$	$n=5$	$n=6$	$n=7$	$n=8$	$n=9$	$n=10$	$n=11$	
183		+1		−1		−1		∓1		±1		Film data
167		+1		−1		−1		∓1		±1		
159		+1		−1		−1		∓1		±1		
165		+1		−1		−1		∓1		±1		Detector data
163		+1		−1		−1		∓1		±1		
161		+1		−1		−1		∓1		±1		
158		+1		−1		−1		∓1		±1		
156 [a]												
149		+1		−1		−1		∓1				
145	−1	+1	±1	−1		−1	−1	−1	−1	−1	−1	
143	−1	+1	±1	−1		−1	−1	−1	−1	−1	−1	

[a] Not phased the intensity of $n = 10$ is $= 0$.

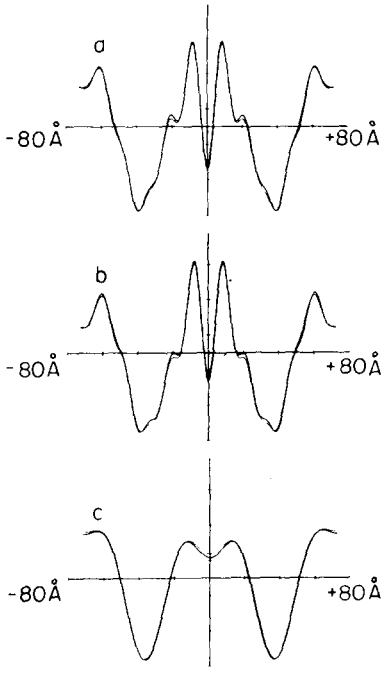

Fig. 6. Electron density profiles for the low periodicity data pair ($d = 143.4$ and 145.3 Å) of Fig. 4 are shown in (a) and (b) for the two best phase assignments. The phases for the orders $n = 1, 2, 3, 4, 6, 7, 8, 9, 10, 11$ ($n = 5$ has negligible intensity) are in (a) $-1, 1, -1, -1, -1, -1, -1, -1, -1, -1$ and in (b) $-1, 1, 1, -1, -1, -1, -1, -1, -1, -1$, respectively. (c) Results if the data are artificially truncated after the 6th order. One division on the abscissa axis corresponds to 20 Å.

the 8th order is strong throughout the entire periodicity range studied and cannot, therefore, have undergone phase reversal over this periodicity range. Based on these considerations alone, we favor the phase choice of Fig. 5a for the high periodicity data.

Profile structure of the rod outer segment disk membrane

We have discussed earlier that we can neither exclude the higher-resolution profile of Fig. 5a nor that of Fig. 5b on the basis of the welling algorithm, therefore, we consider them both as equally probable structures of the rod outer segments disk membrane. Both profiles show two symmetric membrane profiles placed necessarily symmetrically in the unit cell, consistent with our interpretation of the lattice at this periodicity. The profile of Fig. 5a reveals a structure that one would not expect for a simple lipid bilayer containing intrinsic proteins: the two electron density maxima in the single membrane profile have a separatioan of approx. 52 Å and the low density trough appears modified with respect to a fluid lipid hydrocarbon core (see, for instance, Ref. 24). A lipid bilayer profile at 12 Å resolution typically exhibits peaks separated by 40 Å or less, the lipid phosphates being primarily responsible for these features. By contrast, the second of the two profiles (Fig. 5b) shows an electron density distribution for the single membrane characterized by two maxima at $z \approx |20|$ and $|60|$ Å with two relatively high density shoulders centered at $z \approx |11|$ and $|67|$ Å. The profile is similar to that of a lipid bilayer-type membrane with the polar headgroups separated by approx. 40 Å, with extra density due to the presence of presumably the protein protruding in the fluid spaces nearly to the edge of the unit cell, whereafter the density is equal to the average fluid density.

Model calculations, similar to those of Pachence et al. [25] were used to investigate which profile, Fig. 5a or b, might best fit the known physical and chemical data on the disk membrane. In this modelling procedure, one approximates a profile by its step function equivalent. One then, effectively, adds together individual step function profiles of protein lipid and water, subject to the constraint of an assumed lipid to protein ratio, to match the membrane step function profile. This procedure simply accounts for the membrane mass. The assumptions made for the model calculations are the following: rhodopsin is a protein not more than $d/2$ in length and 38000 in molecular weight; the average lipid molecular weight is 800; the rhodopsin/lipid molar ratio is 1 : 65; the membrane profile contains a lipid bilayer whose headgroup spacing is 40 Å. The step function equivalent of Fig. 5a cannot be modelled with the protein to lipid ratio assumed above, unless virtually all the protein is placed in the fluid spaces outside of the lipid headgroup layers, which would seem to contradict the integral membrane protein nature of rhodopsin. However, if one allows the lipid phosphate headgroups to be separated by approx. 50 Å instead of 40 Å in the membrane profile, then a considerably larger fraction of the rhodopsin bulk can be accommodated in the hydrocarbon core of

the lipid bilayer. There is no other evidence of a 50 Å headgroup spacing for the rod outer segment disk membrane, and in fact it might seem unreasonable in view of the average length and high degree of unsaturation of the lipid chains. It is important to note that, even if 'difficult' to model, this profile is the one favored by the diffraction experiments and also that it is more consistent with the profiles at low periodicity. This can be shown by model calcualtions in which one attempts to obtain the step function equivalent of the low periodicity unit cell profile by a suitable overlap of two step function equivalents of the high periodicity membrane profile. If it is assumed that the inter- and intramembrane fluid widths dehydrate at different rates, one can obtain a unit cell profile from two symmetric membrane profiles with relatively higher electron density in one fluid space than in the other, allowing for interdigitation of surface features preferentially in one of the two fluid spaces. No real change in the membrane is required to explain the evolution of the profile (Fig. 5a) at high periodicity into the one at low periodicity (Fig. 6a).

The model calculations applied to the profile of Fig. 5b produce different results: the step function equivalent can be obtained in agreement with all the assumptions listed earlier, including the 40 Å separation of the lipid bilayer headgroups. Choosing slightly different assumed numbers yields somewhat different results, but the fundamental conclusion is that a third or less of the protein is located in the hydrocarbon core and most of it is located in the fluid spaces. Again, the step function equivalent of this membrane profile can be used to model the low periodicity unit cell profiles. As above, the two single membrane profiles are placed asymmetrically in the unit cell in agreement with the assumption of unequal fluid spaces; however, besides interdigitation, more complex changes in the membrane, e.g., significant modification of the protein profile, must occur in this case.

In conclusion, the model calculations do not provide sufficient basis for rejecting one or the other of the profiles of Fig. 5a or b at this time.

At present, the profile of Fig. 5b seems to best fit the known characteristics of the disk membrane components, whereas the diffraction data appears to favor the profile of Fig. 5a. Hopefully, future experiments, such as specific labelling of the lipid headgroups, will resolve these issues.

Further information on the structure of the isolated disk membrane can be obtained by examining the low resolution profiles of Fig. 5c and 6c; they provide a direct comparison (in terms of the resolution) with the profiles derived for the disk membrane in the intact rod outer segment. In the single membrane profile, the peaks are separated by 50 Å. A small degree of asymmatry is present in the profile at lower periodicities. Various studies performed on intact rod outer segments have yielded a consensus view that the membrane profile peaks are spaced about 40 Å apart (see, for instance, Refs. 2, 21 and 26).

We note that prior studies on isolated frog [5,6] and bovine [9] disks have also all yielded profiles in which the peaks are separated by 50 Å or more. Similar dimensions have been derived from analysis of the Patterson functions derived from diffraction of dispersions of isolated frog disks. Thus, the consensus from a wide variety of different isolated disk preparations, hydrations *, methods of data analysis, and at comparable resolution from two different species, indicate that the isolated disk profile is considerably thicker than that in intact rod outer segment. It is of interest to note that upon isolation, peripheral proteins bound to the disk [27] are lost and to speculate that this results in a reorganization of the membrane. This has been observed when cytochrome *c* is bound to reconstituted photosynthetic reaction center membranes [28].

Conclusion

Reproducible, high resolution lamellar diffraction has been obtained from isolated rod outer segment disk multilayers in the absence of lipid phase separation phenomena. Observation of the evolution of the diffraction as the specimen is dehydrated and rehydrated has been used to index

* The membrane thickness does not appear to be affected by the increased concentration of the buffer in the multilayer following dehydration: the low resolution electron density profiles obtained from multilayers sedimented in the presence of buffers at lower concentration (0.1–0.01 M NaCl) are indistinguishable from the profile shown in Fig. 5c.

the diffraction patterns. The diffraction obtained from different states of hydration of single specimens has been used to determine two phase choices for the diffraction and two corresponding electron density profiles for the unit cell. One of the profiles cannot be easily modelled according to the expected chemical and physical characteristics of the disk membrane components, unless one assumes the lipid phosphate groups to reside in two layers approx. 50 Å apart across the membrane profile. This profile is the most consistent with the diffraction data and the profiles at lower periodicity. The other profile is easily modeled with the fraction of rhodopsin in the hydrocarbon core of a third or less, assuming the net lipid headgroup spacing to be approx. 40 Å.

An isolated rod outer segment disk multilayer preparation has been shown to be suitable for high resolution diffraction analysis. Neutron diffraction experiments, combined with X-ray diffraction results, could be used to provide further essential information on the location and structure of the disk components. It should also be possible to examine the disk structure in the presence and absence of the peripheral proteins which are known to interact with rhodopsin and play an important role in vision.

Acknowledgements

We wish to thank George Reynolds for helpful discussions and encouragement. The instrumentation used in this study was supported by the DOE grant DE-AC02-76EV03120. S.M.G. is supported by the NIH grant GM32614. D.P. and J.K.B. were supported by the NIH grant EY00673 (to J.K.B.).

References

1 Olive, J. (1980) Int. Rev. Cytol. 64, 107–169
2 Schwartz, S., Cain, J.E., Dratz, E. and Blasie, J.K. (1975) Biophys. J. 15, 1201–1233
3 Blasie, J.K., Dewey, M.M., Blaurock, A.E. and Worthington, C.R. (1965) J. Mol. Biol. 14, 143–152
4 Blasie, J.K., Worthington, C.R. and Dewey, M.M. (1969) J. Mol. Biol. 39, 407–416
5 Santillan, G. (1975) Ph.D. Thesis, University of Pennsylvania, Philadelphia
6 Hamanaka, T. and Blasie, J.K. (1978) in Diffraction Studies of Biomembranes, Muscles and Synchrotron Radiation, Proceedings of the 4th Taniguchi International Symposium in Biophysics (Mitsu, T., ed.), University of Tsubuka, Ibaraki
7 Gruner, S.M., Rothschild, K.J. and Clark, N.A. (1982) Biophys. J. 39, 241–251
8 Barry, D.T. (1979) Ph.D. Thesis, Princeton University, Princeton
9 Gruner, S.M., Barry, D.T. and Reynolds, G.T. (1982) Biochim. Biophys. Acta 690, 187–198
10 Raubach, R.A., Franklin, L.K. and Dratz, E.A. (1974) Vision Res. 14, 335–337
11 Raubach, R.A., Nemes, P.P. and Dratz, E.A. (1974) Exp. Eye Res. 18, 1–12
12 Stone, W.L., Farnsworth, C.C. and Dratz, E.A. (1979) Exp. Eye Res. 28, 387–397
13 Gruner, S.M. (1977) Ph.D. Thesis, Princeton University, Princeton
14 Reynolds, G.T., Milch, J.R. and Gruner, S.M. (1978) Rev. Sci. Instr. 49, 1241–1249
15 Herbette, L., Marquardt, J., Scarpa, A. and Blasie, J.K. (1977) Biophys. J. 20, 245–272
16 Gruner, S.M. (1981) Rev. Sci. Instr. 52, 134–136
17 Stamatoff, J., Eisenberger, P., Blasie, J.K., Pachence, J.M., Tavormina, A., Erecinska, M., Dutton, P.L. and Brown, G. (1982) Biochim. Biophys. Acta 679, 177–187
18 Stamatoff, J.B. and Krimm, S. (1976) Biophys. J. 16, 503–516
19 Barry, D.T., Costello, M.J. and Gruner, S.M. (1980) Exp. Eye Res. 30, 501–510
20 Henderson, R. (1975) J. Mol. Biol. 93, 123–138
21 Blaurock, A.E. (1975) J. Mol. Biol. 93, 139–158
22 Blaurock, A.E. (1977) in Vertebrate Photoreception (Barlow, H.B. and Fatt, P., eds.), pp. 62–76, Academic Press, New York
23 Rand, R.P. (1981) Annu. Rev. Biophys. Bioeng. 10, 277–314
24 Levine, Y.K. (1973) in Progress in Surface Science (Davison, S.G., ed.), Vol. 3, part 4, pp. 279–352, Pergamon Press, Oxford
25 Pachence, J.M., Dutton, P.L. and Blasie, J.K. (1979) Biochim. Biophys. Acta 548, 348–373
26 Funk, J., Welte, W., Hodapp, N., Wutschel, I. and Kreutz, W. (1981) Biochim. Biophys. Acta 640, 142–158
27 Baehr, W., Devlin, M. and Applebury, M.L. (1979) J. Biol. Chem. 254, 11669–11677
28 Pachence, J.M., Dutton, P.L. and Blasie, J.K. (1983) Biochim. Biophys. Acta 724, 6–19